

Nucleosome repositioning via loop formation

IM . Kulic and H . Schiessel

Max-Planck-Institut für Polymerforschung, Theory Group, P O Box 3148, D 55021 Mainz, Germany
(Dated: October 17, 2021)

Active (catalysed) and passive (intrinsic) nucleosome repositioning is known to be a crucial event during the transcriptional activation of certain eucaryotic genes. Here we consider theoretically the intrinsic mechanism and study in detail the energetics and dynamics of DNA-loop-mediated nucleosome repositioning, as previously proposed by Schiessel et al. (H . Schiessel, J. W idom , R . F . Bruinsma, and W . M . Gelbart. 2001. Phys. Rev. Lett. 86:4414-4417). The surprising outcome of the present study is the inherent nonlocality of nucleosome motion within this model { being a direct physical consequence of the loop mechanism . On long enough DNA templates the longer jumps dominate over the previously predicted local motion, a fact that contrasts simple diffusive mechanisms considered before. The possible experimental outcome resulting from the considered mechanism is predicted, discussed and compared to existing experimental findings.

PACS numbers:

I. INTRODUCTION

The nucleosome, the most abundant DNA-protein complex in nature, is the basic unit of eucaryotic chromatin organization. It is roughly a cylinder of 6nm height and 10nm diameter, consisting of a protein octamer core and 147 basepairs (bp) of DNA tightly wrapped around it in 1 and 3/4 left-handed superhelical turns. The genes of all higher organisms, ranging from simple ones like yeast to most elaborate like humans are all organized in long arrays of nucleosomes with short DNA segments (linkers) of 50-100 bp interpolating between them, comparable to a beads-on-a-string chain [1, 2, 3]. The higher order organization of these units, being most probably a solenoid- or zig-zag, crossed-linker-like fiber with 30 nm diameter is still under great dispute though it received increasing theoretical and experimental support in recent years. Above that scale of organization, the higher order structures which link the 30 nm to the final "big X" like structure, the packed chromosome, are still unknown. Though there are several biologically motivated speculations about the "big X" its definite structure remained a long lasting puzzle for the last 20 years, defying all bio-

physical, biochemical and molecular genetics efforts to resolve it because of its intrinsic softness and fuzziness.

An additional obstacle for understanding the chromatin structure is the fact that it is highly dynamic on all organization scales. Starting at the macroscopic chromosome level we see that its structure can strongly vary throughout the cell cycle on timescales of hours or days. Below that on timescales of seconds and minutes, the structure of the 30 nm fiber itself is subjected to great variations due to transcription, replication, biochemical modification and other dynamic processes. Finally, at the lowest organization level, the nucleosome itself has been shown to be a dynamic structure being moved along the DNA by chromatin remodeling complexes on expense of ATP [4, 5]. Interestingly, it was experimentally observed [6, 7, 8, 9] that nucleosomes can move even autonomously on short DNA segments. This intrinsic repositioning behavior was shown to be strongly temperature dependent. At room temperature it occurs roughly on timescales of

1 hour indicating the existence of significant energetic barriers. Besides the fact that the repositioning does indeed occur and is of intramolecular nature (the nucleosome stays on the same DNA segment) the underlying scenario could not be figured out. It was speculated by Pennings et. al. [8, 9] that the mechanism was some type of nucleosome-sliding or screwing motion. An alternative explanation which appears to be more consistent with the discrete jumps and large barriers observed by Pennings et. al. has been recently proposed in Ref. [10]. In this model the basic step in the repositioning process is a partial unwrapping of DNA from the very ends of the nucleosome [11, 12] followed by a backfolding of DNA with a small 10 bp mismatch (cf. Fig. 1). The result of this process is the formation of a small DNA bulge or loop on the octamer surface. Once trapped on the nucleosome surface this small defect carrying some discrete quantum of DNA extra length (a multiple of 10 bp, the DNA repeat length) can propagate by diffusion in both directions. If the loop happens to surround the nucleosome and comes out at the opposite side (in respect to where it

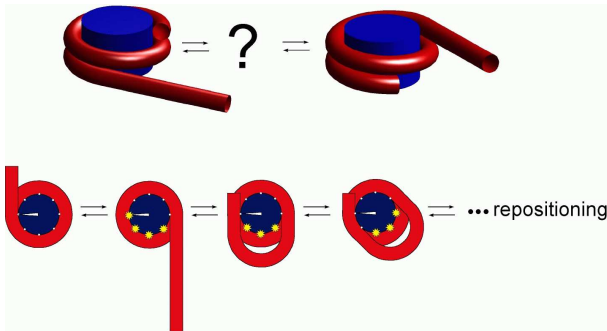


FIG. 1: The basic problem setting: how does the histone-octamer move along the DNA template? Below: the DNA loop mechanism as proposed in Ref. [10]

was created) the nucleosome is eventually repositioned by a distance given by the "pulled in" extra length. The energetic barrier and rates of repositioning were computed and were shown to be consistent with the Pennings et al. experiment [8, 9]. Moreover, the 10 bp discrete step repositioning observed in the experiment (discrete bands, no 1 bp spaced intermediates) came out as a natural consequence of the loop length quantization. The latter is enforced by the strongly preferred DNA minor groove - octamer interaction and the discrete binding sites at the nucleosome surface as deduced from the crystallographic structures [14].

In Ref. [10] small loops with short excess length of typically 1-20 bp were considered and it was shown that the looping energies involved increase rapidly with the excess length implying that only the shortest (10 bp) loop contributes significantly to the repositioning mechanism. Consequently the model predicts a classical discrete random walk with a jump-size of 10 bp instead of a 1 bp motion that would be implied by sliding/corkscrewing mechanism. Apart from the discrepancy in the elementary step size, both models predict very similar behavior: a local one-dimensional diffusive motion along the DNA chain.

In this paper we will carefully reanalyze the idea of loop-mediated repositioning by applying the classical tool of the Kirchhoff kinetic analogy which provides us with analytic solutions of the loop problem and enables us to look at loops of virtually any given excess length. The main outcome of our study will be a different picture of repositioning which physically results from the looping mechanism: on short up to moderately long segments of up to $2-3 \lambda_p$ (λ_p : DNA persistence length) the repositioning is a jumpy process with largest possible loops being the most dominant ones in contrast to short 10 bp steps as conjectured before. For longer and very long (infinite) DNA segments there is an optimal jump size of order $\sim 10 \lambda_p$ and the behavior is superdiffusive in contrast to the previously predicted diffusive mechanism. As we will see below, these predictions allow us to clearly distinguish between different repositioning mechanisms in experiments expected to be performed in near future [13].

II. ENERGETICS OF LOOPS

Let us now consider the energetics of an intranucleosomal DNA loop. We will describe it within the framework of the Euler-Kirchhoff theory for the static equilibrium of rods (Fig. 2). For simplicity and because of the approximate planarity of the problem we can in first approximation assume the nucleosome and the loop-forming DNA to be in one plane and the DNA to be free of any twisting deformation. In this case the free energy of our system is simply divided into two components, the planar elastic DNA-bending and a histone-octamer DNA interaction:

$$U_{\text{tot}} = U_{\text{bend}} + U_{\text{ads}} \quad (1)$$

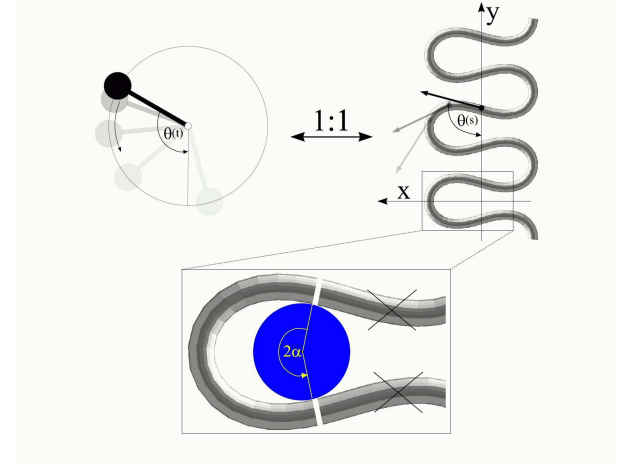


FIG. 2: The Kirchhoff kinetic analogy between the spinning top and the bent/twisted rod depicted for a special case: the plane pendulum - planar rod equivalence. The inset shows how an intranucleosomal loop can be constructed by inscribing the octamer (gray disk) into the bent rod. The nucleosome opening angle 2α accounts for the adsorption energy cost (see text for details).

The bending energy (within the linear elasticity approximation) can be written in terms of the local DNA curvature

$$U_{\text{bend}} = \frac{A}{2} \int_{L=2}^{L=L} \kappa^2(s) ds \quad (2)$$

with $A = 50 \text{ nm}^2 k_B T$ being the bending rigidity of DNA at room temperature and physiological salt concentrations [15]. The rod is assumed to be parameterized by its contour length parameters ranging from $L=2$ to $L=L$ with L being the total length of the loop. The latter can be expressed in terms of two independent quantities: the excess length L and the nucleosome opening angle (Fig. 2)

$$L(\alpha; L) = 2R + L \quad (3)$$

where $R = 4 \text{ nm}$ is the effective nucleosome radius, or more precisely the distance from the center of the nucleosome to the central DNA axis. Because the DNA can enter the nucleosome only in quantized orientations (with its minor groove phosphates) and bind only to discrete positions on the protein surface [14], the excess length $L = n h_{\text{DNA}}$ is to a good approximation an integer multiple of the DNA repeat length $h_{\text{DNA}} = 3.4 \text{ nm}$.

The second part in the total energy Eq. 1 U_{ads} comes from the (predominantly electrostatic) interaction between the positively charged protein surface and the negatively charged DNA. It can be roughly measured from experiments probing the competitive protein binding to nucleosomal DNA [11, 12]. Neglecting the discreteness of charges (binding sites) on the histone octamer surface it can in first approximation be assumed to be proportional

to the opening angle θ and the adsorption energy density U_{ads}

$$U_{\text{ads}} = 2 R \theta_{\text{ads}} \quad (4)$$

with $\theta_{\text{ads}} = 0.5 - 1.0 \text{ kT/nm}$ as roughly extracted from [11]¹. Here and in the following we assume an intermediate value of $\theta_{\text{ads}} = 0.7 \text{ kT/nm}$.

A. Ground states of trapped loops

In order to compute the ground state for a trapped intranucleosomal loop we have to consider shapes that minimize the total energy Φ under two constraints:

1. The excess length L is prescribed. Therefore we have the relation Eq. 3 between the opening angle and the total loop length L

$$L = L_0 - 2 R \theta = \text{const:} \quad (5)$$

2. At the two ends $s = L/2$ the rod has to be tangential on an inscribed circle of given radius (representing the nucleosome)²:

$$R = \frac{y \frac{L}{2}}{x'^0 \frac{L}{2}} = \text{const:} \quad (6)$$

Here $x(s)$ and $y(s)$ are the Cartesian coordinates of the rod axis as a function of the arc-length parameter s (cf. Fig. 2). The absolute value in the second constraint needs to be introduced formally for dealing with crossed rod solutions (which we consider later on) and can be omitted for simple uncrossed loops.

For an analytical description it is convenient to use the angle $\theta = \theta(s)$ between the DNA tangent and the y axis (cf. Fig. 2) as a variable describing the DNA centerline. In this case the integrated sine (cosine) of θ over the arc-length parameters gives the x (y) Cartesian coordinate of any point along the rod, and the squared derivative $(\theta')^2$ gives the rod curvature. Furthermore the nucleosome opening angle θ is simply related to θ at the boundary

$$\theta = \begin{cases} \theta_{\text{ads}} & (L=2) \text{ for simple loops} \\ \theta_{\text{ads}} + \pi & (L=2) \text{ for crossed loops} \end{cases}$$

The two constraints Eq. 5 and Eq. 6 can be rewritten in terms of θ and then be introduced into the minimization

by two Lagrange multipliers $\lambda_1 = \lambda_2$. We then arrive at the following lengthy functional

$$\begin{aligned} \Phi_{\text{tot}} = & A \int_0^{L/2} (\theta')^2 ds + 2 R \theta_{\text{ads}} \\ & + \lambda_1 [L - (L_0 - 2 R \theta)] \\ & + \lambda_2 \int_0^{L/2} \cos \theta ds - R \sin \theta \end{aligned} \quad (7)$$

Here the first line is the bending + adsorption energy contribution, the second and third line are the imposed length and tangency constraint. Eq. 7 can be rearranged in a more familiar form

$$\int_0^{L/2} A (\theta')^2 + \lambda_2 \cos \theta ds + \text{b.t.} \quad (8)$$

Here b.t. denotes the boundary terms (depending on $L=2$ only) that obviously do not contribute to the first variation inside the relevant s interval. The integral in Eq. 8 is evidently analogous to the action integral of the planar pendulum with $A (\theta')^2$ corresponding to the kinetic and $\lambda_2 \cos \theta$ to the potential energy of the pendulum. The latter analogy is a rather unspectacular observation knowing the celebrated Kirchhoff's kinetic mapping between deformed rods and the spinning top, which contains our present problem as a simple special case. The Kirchhoff's analogy states that the equilibrium conformations of (weakly) deformed thin rods can be mapped to the time-dynamics of a heavy symmetric spinning top subjected to a gravitational force. It has been repeatedly applied (with or without direct reference to Kirchhoff) to DNA related problems during the last 20 years (e.g. see [16, 17, 18, 19, 20, 21, 22, 23, 24]). For a nice visual review on the spinning top-elastic rod analogy the reader is referred to Ref. [25] where the general solutions together with a "kinetic dictionary" (time \leftrightarrow length parameter s , gravitational force \leftrightarrow rod tension λ_2 , axis of revolution \leftrightarrow tangent vector etc.) are also provided.

The nice thing about Kirchhoff's analogy apart from its esthetical content is that it provides us with explicit expressions for DNA shapes subjected to twist, bending and various geometric / topological constraints. In our simple planar and twistless case, the "spinning top" simply reduces to the simple plane pendulum. The corresponding planar and twistless rods, also called the Euler elastica, are most generally given by

$$\cos \theta(s) = 1 - 2m \sin^2 \frac{s}{2} \quad (9)$$

which can be integrated to obtain the general planar rod shape in Cartesian coordinates:

$$x(s) = 2 \frac{R}{m} \text{cn} \frac{s}{2} \quad (10)$$

$$y(s) = 2 R E \frac{s}{2} - R \text{sn} \frac{s}{2} \quad (11)$$

¹ In Eq. 4 we assume that the interaction is only short ranged (contact interaction) which is justified by the very short Debye screening length of $\approx 1 \text{ nm}$ under physiological salt conditions.

² Because of the symmetry we have to impose the conditions only on one side.

with $\text{sn}, \text{dn}, \text{cn}(\cdot; m)$ being the Jacobi elliptic functions with the parameter m and

$$E(u; m) := \int_0^u \text{dn}^2(v; m) dv \quad (12)$$

denoting the incomplete elliptic integral of the second kind in its "practical" form³. The two parameters $m > 0$ and $u > 0$ in Eqs. 10, 11 characterize the shape and the scale of the solution, respectively. These solutions are up to trivial plane rotations, translations, reflections and shifting of the contour parameter $s \rightarrow s + s_0$ the most general planar Euler elastica corresponding to the plane pendulum. For different parameters m one obtains different rod shapes corresponding to different solutions of the spinning top (plane pendulum) motion [25]. The case $m = 0$ describes a pendulum at rest corresponding to a straight rod, for $0 < m < 1$ one has strictly oscillating pendulums corresponding to point symmetric rod shapes which for $m < 0.92$ are free of self-intersections like the one depicted in Fig. 2. For m higher than 0.92 the rods show varying complexity with a multitude of self-intersections and for $m = 1$ one has the so-called homoclinic pendulum orbit corresponding to a rod solution having only one self-intersection and becoming asymptotically straight for $s \rightarrow \pm 1$ (for details see Ref. [25]). For even higher values⁴ of m , i.e., for $m > 1$ we have revolving pendulum orbits corresponding to rods with self-intersections lacking point symmetry. Finally, the limiting case $m \rightarrow \infty$ corresponds to the circular rod shape.

In order to describe a trapped loop we need to use Eqs. 10 and 11 imposing the constraints Eq. 5 and Eq. 6. It turns out to be more convenient to replace the parameter set $(\cdot; m; L)$ with the new (but equivalent) set $(\cdot; m; \kappa = \frac{L}{2})$ where we introduced the new dimensionless parameter κ which we call the "contact parameter"⁵. From Eq. 6 together with 10 and 11 we can immediately extract the scaling parameter R and the opening angle in terms of the contact parameter κ and the shape parameter m

$$R(\cdot; m) = R \frac{\text{sn}(\cdot; m) \text{dn}(\cdot; m)}{2E(\cdot; m)} \quad (13)$$

$$\kappa(\cdot; m) = \arccos \frac{2\text{dn}^2(\cdot; m) - 1}{2} \quad (14)$$

$$\sigma = \text{sign}(2E(\cdot; m) - \kappa) \quad (15)$$

Plugging this into Eq. 5 we obtain the final form of the implicit constraint

$$\frac{L}{2R} = \frac{\text{sn}(\cdot; m) \text{dn}(\cdot; m)}{2E(\cdot; m)} \arccos \frac{2\text{dn}^2(\cdot; m) - 1}{2} \quad (16)$$

The curvature $\kappa(s)$ and the bending energy Eq. 2 follow from the explicit solution Eq. 9 to be

$$\kappa(s) = \frac{2\sqrt{m}}{Z} \text{cn} \left(\frac{s}{Z}; m \right) \quad (17)$$

$$U_{\text{bend}} = \frac{4mA}{Z} \int_0^Z \text{cn}^2(t; m) dt \quad (18)$$

$$= \frac{4A}{Z} [E(m) - (1-m)E(\cdot; m)] \quad (19)$$

The latter expression together with Eqs. 1, 4 – gives a lengthy expression for the total energy with the sign chosen as in Eq. IIIA.

$U_{\text{tot}}(\cdot; m) =$

$$\frac{4A}{R} \frac{[2E(\cdot; m) - \kappa]E(\cdot; m) + (m-1)\kappa}{\text{sn}(\cdot; m) \text{dn}(\cdot; m)} + 2R \kappa_{\text{ads}} \arccos \frac{2\text{dn}^2(\cdot; m) - 1}{2} \quad (20)$$

Now our problem of finding the ground state loop for given excess length L reduces to a two variable $(\cdot; m)$ minimization of Eq. 20 under the constraint Eq. 16. This final step is easily performed numerically.

III. LOOP ZOOLOGY: SIMPLE AND CROSSED LOOPS

We can scan now through the m parameter plane and look at the shapes of the solutions and their energies. In Fig. 3 we see a small (but most important) part of the whole parameter space and the corresponding different loop geometries. The dashed lines indicate parameter values which lead to constant excess length $L = 10 \pm 3.4 \text{ nm}$ (corresponding to 100 bps) in accordance with the constraint Eq. 16. The shapes 1-7 are examples of 100bp-loops with different geometries. The whole parameter plane is subdivided by separation lines (solid) into regions of structurally different solutions. The large region starting at $\kappa = 0$ contains exclusively simple loops (like 1, 2 and 3) without self-intersections and nucleosome penetration. Above that simple-loop-region we find loops with a single self-intersection (4, 5, 6) and to the right the loops penetrate the nucleosome, like loop 10. There are also three other regions with single and double crossing points (7, 8, 9) where the loop can also be on the "wrong" side of the nucleosome like in 7 and 8.

We are interested in the energy minimizing loops and the underlying minimal energies as functions of the excess length L . A density plot of these energies as function

³ Some useful formulas and relations for the elliptic functions and integrals are briefly sketched in [25] and found in [26] in full depth.

⁴ Usually the parameter m is artificially assumed to be confined to $0 < m < 1$ but by the Jacobi's real transform for elliptic functions [26] they stay well-defined even for $m > 1$.

⁵ A more visual parameter set $(\cdot; m; \kappa)$ using the opening angle $\kappa = \kappa(\cdot; m)$ produces technical problems with non-uniqueness of loop representation.

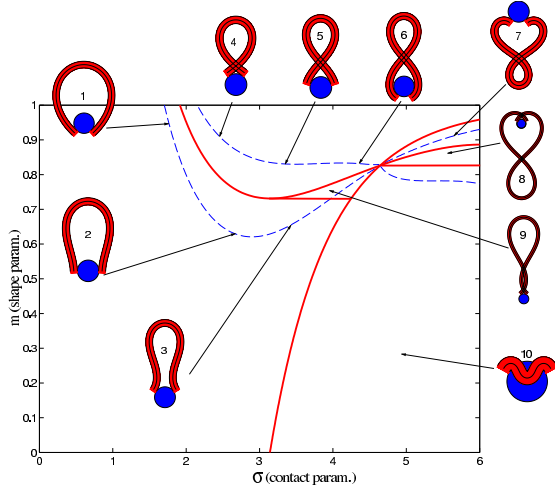


FIG. 3: The set of possible ground-state solutions is characterized by two parameters, the contact point parameter σ and the loop shape parameter m . Solutions with constant excess length L (here $10 \text{--} 3.4 \text{ nm}$) are located along the dashed lines (e.g. loops 1–7). The solid lines separate loops with different geometric characteristics: simple (1,2,3), crossed (4,5,6) and "exotic" (7,8,9,10) loop shapes.

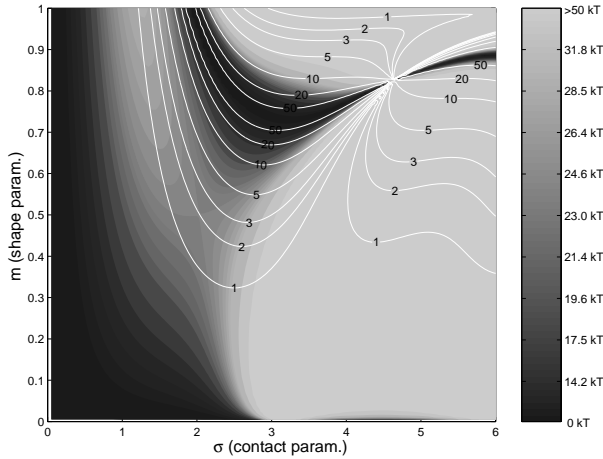


FIG. 4: Density plot of the total loop energy Eq. 20 (grayscale levels) as a function of σ and m (same parameter range as in Fig. 3). The white contours denote lines of constant excess length $L = 1; 2; 3; 5; 10; 20; 50 \text{--} 3.4 \text{ nm}$. For given excess length the ground state is the point on the corresponding white line with the darkest background (note the different branches for given L). The parameters are $\mu_{\text{ads}} = 0.7 k_B T = \text{nm}$ and $A = 50 \text{ nm}$, $k_B T$ and $R = 4 \text{ nm}$.

of the parameters σ and m together with the corresponding lines of constant L (with $L = 1; 2; \dots; 50 \text{--} 3.4 \text{ nm}$) is given in Fig. 4. As can be seen from Fig. 3 there are, for a given L , different branches of $(\sigma; m)$ values corresponding to uncrossed, simply crossed and other exotic structures. Of all these structures for short excess lengths, $L < 20 \text{--} 3.4 \text{ nm}$, the energetically dominant

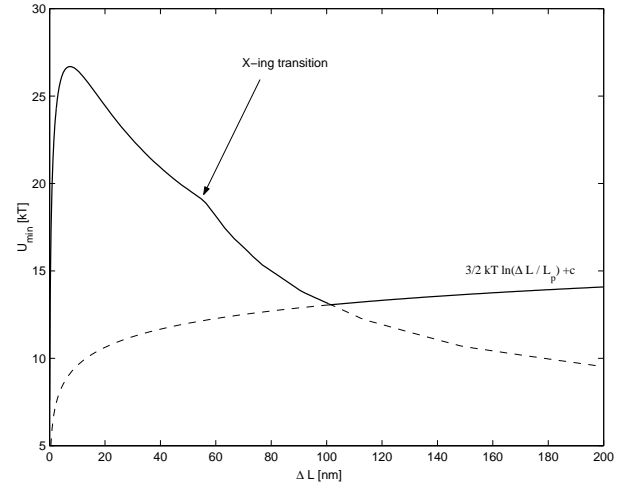


FIG. 5: The ground state loop energy plotted vs the excess length L . Note the energy maximum occurring for shorter loops. For much longer loops (around $L = 60 \text{ nm}$) a transition from simple uncrossed to crossed loop shapes leading to a kink in $U_{\text{min}}(L)$. In the regime of low $L < L_p$ the elastic energy prevails strongly over entropy whereas for large loops the entropy starts to dominate the behavior producing a shallow energy minimum in the cross-over regime which roughly defines the predominant loop size.

ones are simple (uncrossed) loops which we study first. Loops with larger excess length form crossed structures and are studied in Section 3.2.

A. Simple Loops

For simple uncrossed loops it is a straightforward numerical task to minimize Eq. 20 under the constraint of constant excess length, Eq. 16. For $\mu_{\text{ads}} = 0.7 k_B T = \text{nm}$ and all the other parameters as above ($A = 50 \text{ nm}$, $k_B T$; $R = 4 \text{ nm}$) the ground state energy U_{min} as a function⁶ of the excess length L is shown in Fig. 5 (for $L < 60 \text{ nm}$; for longer L -values crossed loops are more favorable as discussed in the next section). Remarkably we find that the loop energy is non-monotonous: For small L U_{min} increases with L as $(L)^{1/3}$ (in accordance with Ref. [10] where only small loops were studied). At some critical excess length $L = L_{\text{crit}}$ (which is approximately $L_{\text{crit}} \approx 2.2 \text{--} 3.4 \text{ nm}$ for $\mu_{\text{ads}} = 0.7 k_B T = \text{nm}$) the loop energy reaches a maximum (here $U_{\text{min}}(L_{\text{crit}}) \approx 26 k_B T$). Beyond that the energy decreases with increasing L .

In the following we show how this behavior can be explained on the basis of the loop geometry. Naively

⁶ Formally the quantisation condition $L = 1; 2; \dots; 3.4 \text{ nm}$ holds as mentioned above. Nevertheless for clarity we consider the values in between as well.

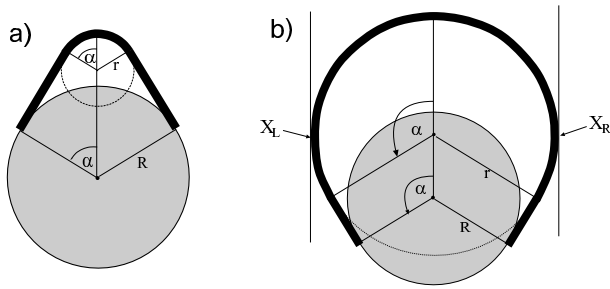


FIG. 6: Two generic types of simple loop geometries (in the circle-line approximation): a) the subcritical loop with opening angle ≤ 2 and b) the supercritical loop with ≥ 2 . In the former case the introduction of further excess length leads to an energy increase but in the latter case to a relaxation of stress: The introduction of additional length at points X_L and X_R followed by a relaxation of the structure obviously decreases the total energy.

one might argue as follows: For excess lengths shorter than the persistence length of DNA it is increasingly difficult to store additional length into the loop because it requires increasing DNA deformation. On the other hand, for loops longer than l_p the bending energy contribution becomes very small and hence one expects such ground state loops relaxing with increasing L . However the reason for occurrence of a maximum of U_{min} around

2 excess DNA lengths, a value which is considerably smaller than the persistence length, is not obvious. In order to understand this finding one has to go beyond the simple handwaving heuristics and needs to take a close look at the details of the loop geometry.

To this end we introduce here a simple approximation technique which leads to explicit expressions which can be more easily handled than the exact yet complicated expressions given above. We call this method the circle-line approximation and give a detailed exposition in the Appendix. As we will see this method is quite accurate and at the same time very intuitive.

Looking at the geometrical shapes of the loops in Fig. 3 we notice that each of them is subdivided into several sections of very high and very low curvature (cf. also Eq. 17). In first approximation we replace the high curvature regions by sections of circles, the low curvature regions by straight lines (cf. Fig. 6). Furthermore, to keep the smoothness we assume that the lines are tangents to the circles. Generally in order to have reasonable approximations of all possible loop shapes we would need to consider compositions of several circles and lines (cf. for instance loops 3, 6, 7). However, if the adsorption energies are not too high, i.e., if the opening angle is "soft enough" and does not impose such a severe bending like in loop 3, such multiply bent loops will not be relevant as ground state solutions. As it turns out for our problem we already obtain a quite good approximation by assuming that the loop consists of a single circular arc and two lines only. It is characterized by two quantities: 1) the arc radius r and 2) the nucleosome opening angle (cf.

Fig. 6 and Appendix). With these assumptions and after some elementary geometry the constraint Eq. 5 becomes simply

$$L = 2(R - r)(\tan \frac{\alpha}{2}) = \text{const:} \quad (21)$$

Note that the (more complex) second constraint Eq. 6 is eliminated through the "ansatz" per se. The total loop energy is given in terms of the loop radius r and the opening angle

$$U_{tot}(\alpha; r) = A \frac{1}{r} + 2R \epsilon_{ads}$$

and by applying the constraint Eq. 21 (which this time can be solved explicitly!) we obtain U_{tot} in terms of L and given L

$$U_{tot}(L) = 2A \frac{\tan \frac{\alpha}{2}}{2R(\tan \frac{\alpha}{2})} + R \epsilon_{ads} \quad (22)$$

which is explicit in L . We note that this approximation for U_{tot} is only reasonable for $2R(\tan \frac{\alpha}{2}) > L$, i.e., for not too small α (vs. L), otherwise the bending contribution diverges or becomes even negative (the latter is obviously absurd). The reason for this is that for very small angles α (compared to L) uncrossed⁷ circle-line loops cannot exist for geometrical reasons. There this most basic approximation breaks down and we would have to approximate the loop by more than one circular segment. But as mentioned above, such loops (small α compared to L) are not candidates for the ground state for moderate $\epsilon_{ads} \ll 0(1)$, and we therefore dispense with giving a discussion of this case.

The nice thing about Eq. 22 is that despite its simplicity and approximate nature it reproduces the position of the maximum in Fig. 5 quite well. We find the condition for the critical excess length L_{crit} from a simple geometric distinction between two loop shapes: the subcritical loop (Fig. 6a) with its tangents not being parallel to the Y axis ($\alpha = 0$) and the supercritical loop (Fig. 6b) having two or more tangents parallel to the line $\alpha = 0$. Suppose now we add excess length to a subcritical loop by keeping the angle $\alpha = \text{const}$. Obviously the loop-energy increases because the loop radius r becomes smaller. On the other hand in the supercritical case we have the opposite situation: the loop energy decreases with increasing L .

This is simply because we could cut the loop at two points (X_L and X_R in Fig. 6), introduce there the additional length (without changing the energy) and then relax the shape by letting it evolve to the new equilibrium while keeping $\alpha = \text{const}$. Thus we can obtain the condition for the critical excess length L_{crit} by assuming that the corresponding minimum U_{min} of U_{tot} just crosses

⁷ In contrary for crossed loops there still are solutions for small α (cf. next chapter).

the critical line $=2$ line, i.e., $\min L^{\text{crit}} = 2$ for the searched L^{crit} .

$$\frac{d}{d} U_{\text{tot}}(\cdot) \stackrel{!}{=} 0 \quad (23)$$

which can be solved for L^{crit}

$$L^{\text{crit}} = \frac{4R}{A} + \frac{8R^3}{A} \mu_{\text{ads}} \quad (24)$$

The latter can now be inserted in Eq. 22 leading to

$$U_{\text{tot}}^{\text{crit}} = \frac{A}{2R} + R \mu_{\text{ads}} \quad (25)$$

For the given values of R ; A ; μ_{ads} ($R = 4\text{nm}$, $A = 50\text{nm k}_B T$, $\mu_{\text{ads}} = 0.7\text{ k}_B T = \text{nm}$) we obtain $L^{\text{crit}} = 7.37\text{nm}$ and $U_{\text{tot}}^{\text{crit}} = 28.4\text{ k}_B T$ which is in satisfactory agreement with the exact numeric results ($L^{\text{crit}} = 7.19\text{nm}$, $U_{\text{tot}}^{\text{crit}} = 26.7\text{ k}_B T$). More generally, for not too high adsorption energies ($\mu_{\text{ads}} = 0.5 - 2.0\text{ k}_B T = \text{nm}$) the circle-line approximation works well and Eqs. 24 and 25 reproduce the exact positions of the critical point typically with a 5-15% accuracy.

For an explicit parametric representation of the minimal energy curve within the circle-line approximation, which in particular implies the upper results, the reader is referred to the appendix where the usefulness of this approach is also demonstrated for some other examples.

B. Crossed and Entropic Loops

A closer inspection of Fig. 4 shows that the ground state of loops switches from simple uncrossed loops to crossed loops when one reaches an excess length around 50nm . However, as can be seen for the crossed structures 4, 5 and 6 in Fig. 3 these loops have a self-penetration at the crossing point. Therefore, a planar theory is in principle not sufficient to describe such structures. One possible formal cure for this problem would be to leave the plane and to consider the rod's self-contacts with the corresponding point-forces etc. in 3D as done by Coleman et al. in a general theory of rod self-contacts [27]. However such a procedure leads to a significant loss of transparency, not only because of the third dimension entering the scene but also due to the necessity to subdivide the rod into different regions with different forces acting in each of them. Instead of following Coleman et al. [27] we decided to treat the self-interaction in a perturbative manner as follows. If the self-contact point is not too close to the nucleosome the rod is not severely deflected out of the plane by its self-interaction. Thus it remains roughly planar with some out of plane bending in Z -direction of the rod sections between the nucleosome and the crossing point. This will cost some additional bending energy U_{def} that is roughly given by (cf. Appendix)

$$U_{\text{def}}(\cdot; m) = \frac{2A}{R} \frac{\arctan \frac{\tan(\cdot; m)}{\tan^2(\cdot; m)^2}}{\tan^2(\cdot; m)^2} \quad (26)$$

Here $\cdot = d=R$ with $d = 1\text{nm}$ is the DNA radius. We neglect the slight twisting of the rod induced by the non-planarity of the DNA and consider the bending only. The deflection energy Eq. 26 can be phenomenologically incorporated into the model by simply adding it to Eq. 20 as a correction term to obtain the final form of the total energy U_{tot}

$$U_{\text{tot}}(\cdot; m) = \begin{cases} U_{\text{tot}}(\cdot; m) & \text{for uncrossed (simple) loops} \\ U_{\text{tot}}(\cdot; m) + U_{\text{def}}(\cdot; m) & \text{for crossed loops} \end{cases}$$

With this additional modification of U_{tot} we computed numerically the minimal energy (ground state) solution for any given excess length L . The graph of the ground state energy versus L is shown in Fig. 5. We find that even with the inclusion of the out-of-plane deflection there is still a critical length L_{cross} (here 60nm) where the crossed loops become energetically more favorable than the simple uncrossed. This behavior that we call the "crossing transition" can be rationalized by noting that for long enough loops the adsorption energy (proportional to L) starts to dominate over the bending energy so that loops with smaller L become increasingly favorable. From the critical length L_{cross} on, the gain in adsorption energy (by diminishing L) is more than sufficient to outweigh the (slight) increase in bending energy together with the additional self-interaction term, Eq. 26.

Increasing the length even further we leave the elastic energy dominated regime in which the entropic effects can be neglected due to short loop length ($<$ persistence length). For larger lengths entropic effects become more and more important and we ultimately enter the entropic loop regime. The crossover between these two regimes is hard to handle analytically [28]; for the case of closed loops a perturbative description has been given in Ref. [29]. For our purpose it is sufficient only to consider the asymptotic behavior. In the large loop limit where the loop is longer than several λ_p the chain loses its "orientational memory" exponentially and behaves roughly as a random walk which starts from and returns to the same point. The entropic cost for gluing the ends of a random walk (long loop) together is then given by

$$U = 3 = 2k_B T \ln(L/\lambda_p) + E_0 + S_0 \quad (27)$$

The first constant, $E_0 = 6.5\text{ k}_B T$ is the bending + adsorption energy contribution of the overcrossing DNA segments leaving / entering the nucleosome which can be determined by minimizing the crossed loop energy (cf. Appendix Eq. 31) for $L \gg 1$. The second additive constant $S_0 = 0\text{ (k}_B T)$ accounts for the entropic contribution of DNA-histone octamer interaction volume (the proximity necessary for the histone octamer and DNA to see each other). Although the latter constant is not easy

to estimate the following prediction is not sensitive to any additive constant. We expect a free energy minimum to occur at the overlap between the elastic ($L < l_p$) and entropic ($L > l_p$) region where the decreasing elastic energy is overtaken by the increasing entropic contribution.

The free energy, Eq. 27, leads to an algebraically decaying probability $w(L)$ for the jump lengths scaling as $w(L) \sim L^{-3/2}$. In general, power law distributions of the form $w(L) \sim L^{-\alpha}$ with $\alpha > 1$ lead to superdiffusive behavior of the random walker (here the nucleosome). According to Levy's limit theorem the probability distribution of the random walker (more precisely, the distribution of the sums of independent random variable drawn out from the same probability distribution $w(L)$) converges to a stable Levy distribution of index $1/\alpha$ [30, 31, 32]. This so-called Levy-flight differs in many respects from the usual diffusion process as for short time intervals big jumps are still available with significant probability. Moreover, all moments (besides possibly the first few ones) diverge. For our case $\alpha = 3/2$ even the first moment does not exist. We note that the value $3/2$ is based on the assumption of an ideal chain (no excluded volume); in general the excluded volume leads to self-avoiding-walk statistics with a slightly larger value of α around 2.2 [32] (cf. also Ref. [33]). In that case one has a finite value of the first moment, i.e., of the average jump length.

IV. THE DYNAMICS OF NUCLEOSOME REPOSITIONING

In the preceding sections we have computed the typical energies involved in the formation of arbitrary sized loops. Assuming that a slow creation followed by a fast terminal migration of loops around the nucleosome is the governing mechanism for nucleosome repositioning we start now considering the repositioning dynamics. In order to describe the time-dependent evolution of the nucleosome position we consider its probability distribution along a DNA segment of a length $N = 10$ bp and write the master equation governing the jump process

$$\frac{d}{dt} p_i = \sum_{j=1; j \neq i}^N w_{ji} p_j - p_i \sum_{j=1; j \neq i}^N w_{ij} \quad (28)$$

where p_i is the probability for the nucleosome being at the admissible⁸ position i on the DNA segment. The transition rate matrix $\underline{W} = (w_{ij})$ is given by

$$w_{ij} = \begin{cases} C_A \exp \left(-\frac{1}{k_B T} U_{\min}(h_D |i-j|) \right) & \text{for } i \neq j \\ \sum_{k=1; k \neq i}^N w_{ik} & \text{for } i = j \end{cases} \quad (29)$$

⁸ Spaced by a multiple of 10 bp from the initial position

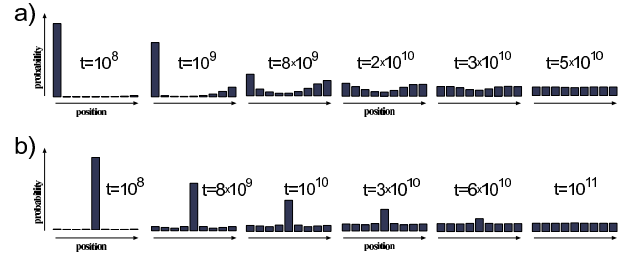


FIG. 7: Relaxation dynamics of two initial states of nucleosome positions on a short DNA segment (147 + 90 bp): a) the nucleosome starting from an end and b) the nucleosome starting from the middle position. The time unit is the inverse Arrhenius activation factor C_A^{-1} (compare text).

where $h_D = 3.4$ nm (DNA helical pitch). C_A denotes the Arrhenius constant involved in the loop formation process that has in principle to be determined experimentally. The rough estimate of $C_A^{-1} = 10^6$ s is provided in Ref. [10] where it was shown that C_A is essentially given by the inverse lifetime of the loop (denoted by A in that paper). This means that typical repositioning times range from seconds to hours.

The (formal) explicit solution of Eqs. 28, 29 together with the previously obtained minimal energy U_{\min} is given by

$$\underline{p}(t) = \exp(\underline{W}t) \underline{p}(0)$$

The latter solution can now be considered for different cases: for short or long DNA chains and for the nucleosome placed in the middle or at the end of the chain.

For short DNA segments we expect a slow repositioning rate due to high energies involved in small loop formation. In Fig. 7 we depict the repositioning of a nucleosome on a DNA piece of a length 147 + 90 bp. Starting from an end-positioned nucleosome (Fig. 7a) we observe a behavior that is completely unlike a local diffusion mechanism: the jumps bigger than 2×3.4 nm start to dominate over the smaller local ones, which follows from the loop formation energy cf. Fig. 5. Consequently, in the initial phase of repositioning (of such an end-positioned population) the nucleosomes will predominantly jump between the two end positions. Later, on a much larger timescale they gradually start to explore the positions towards the middle of the DNA segment. Could we extract such a behavior from an experiment using gel-electrophoretic separation (as in [8], [9])? The basis of such separations is the fact that the gel-electrophoretic mobility of nucleosomes on DNA pieces (longer than 147 bp) increases roughly linearly with its distance from the middle position, i.e., DNA pieces with the nucleosome sitting close to the end run much faster in gels than equivalent middle-positioned nucleosomes do. We can exploit this (empirical) fact to mimic the outcome of a gel-electrophoresis experiment (cf. Figs. 8 and 10). In Fig. 8a we depict such a simulated gel pattern for the

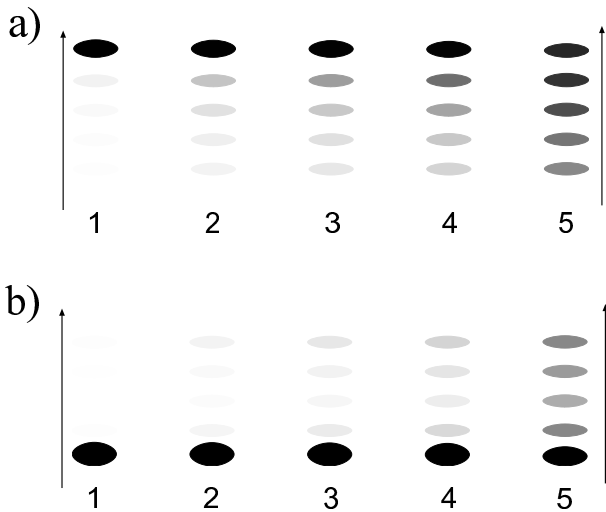


FIG. 8: Typical (1-D) gelelectrophoresis signatures expected for the relaxation dynamics of the two species from Fig. 7: a) nucleosome starts from an end and b) from the middle position. The lanes 1-5 correspond to incubation times $(1, 5, 10, 20, 100) \cdot 10^8 C_A^{-1}$ respectively. Note: the population of distant bands in b) lanes 2-4 occurs first, in sharp contrast to what we expect from a simple (local) diffusive behavior.

middle positioned nucleosome. Since symmetric species are not distinguished by this experimental method and are projected onto the same bands (symmetric left/right positions lead to the same mobility), the expected non-locality of motion cannot be extracted from the structure of the bands.

For the same short segment, but with the nucleosome starting from the middle position (Fig. 7b) the situation is slightly different: the neighboring positions are populated more homogeneously, although there is a small initial underpopulation of the $2-3.4$ nm distant position as expected from the energy maximum occurring there. In this case, a slight initial "population gap" can be observed in gelelectrophoresis (Fig. 8b) which in this case would be sufficient to distinguish between a jumpy and a diffusive behavior, since the latter would obviously lack the "population gap".

In the case of longer DNA (but still not entropic segments) like the $147+300$ bp segment in Figs. 9 and 10, similar effects as for the short segments are expected but with significantly faster relaxation times by typically 2-3 orders of magnitude as compared to the corresponding short segment populations. The corresponding (simulated) electrophoretic gels are shown in Fig. 10 where for the centrally positioned case (Fig. 10b) the "population gap" effect is even more pronounced than in the short segment case.

For even longer DNA segments we expect the gap effect to persist (data not shown) and the optimal jump size to be around $2-3 \lambda$ corresponding to the free energy minimum in Fig. 5. For very long DNA segments, the nucleosome repositioning behavior implied by the big-loop-

mechanism becomes strongly non-local which contrasts a local diffusive motion as expected from cork-screwing motion (cf. Refs. [6, 7, 8, 9]) or small loop repositioning as considered by Ref. [10]. As mentioned above, this superdiffusive behavior has diverging moments which implies strongly enhanced nucleosome transport along very long DNA pieces. However such an ideal superdiffusion of nucleosomes could hardly occur in vivo because free DNA segments between subsequent nucleosomes (DNA linkers) are never longer than 10λ . Furthermore the neighboring nucleosomes might be a significant barrier (if not for loop formation then) for loop migration around the nucleosome which is an indispensable event for loop-mediated repositioning.

V. CONCLUSIONS AND DISCUSSION

In this study we examined a possible mechanism for the repositioning of nucleosomes along DNA which is based on the formation and diffusion of intranucleosomal loops. The most important outcome of this study is the prediction of two classes of loops that might occur: (1) small 10bp-loops and (2) large loops with a wide distribution of stored lengths with a weak peak at roughly two times the DNA persistence length.

The small loops were already discussed in Ref. [10] and led to the prediction of repositioning steps of 10bps. Furthermore, the repositioning time should be of the order of an hour, a consequence of the large activation energy required to form a loop. This might explain the strong temperature dependence of the typical repositioning time [8]. In fact, by lowering the temperature from 37 to 4 C no redistribution within one hour was detected in that experiment. Assuming a loop formation energy of $23 k_B T$ one finds indeed a slowing down of this process by factor of 13.

On the other hand, the large loop repositioning considered here turns out to be energetically much more favorable. Loops with an extra length of 2λ have an energy that is roughly $12-13 k_B T$ smaller than that of a 10bp-loop. To a certain extent this is because such loops can have a very small nucleosome opening angle by forming crossed loops but the main contribution stems from the significantly decreased DNA bending energy. One therefore expects that repositioning via large loops should be the dominant process on sufficiently large DNA pieces and that the typical times are much shorter than the one for small loop repositioning (say, of the order of minutes).

So far, however, the experiments did not report such events. Meersseman et al. [8, 9], for instance, found on short DNA pieces of 207bps length results that are consistent with 10bp repositioning (as we would expect for such short DNA fragments). However, when they redid the experiment with a 414bp long piece, a tandem repeat of the 207bp DNA, their analysis of the complicated band patterns observed in 2D gelelectrophoresis did not show any indication that the nucleosome was able to move from

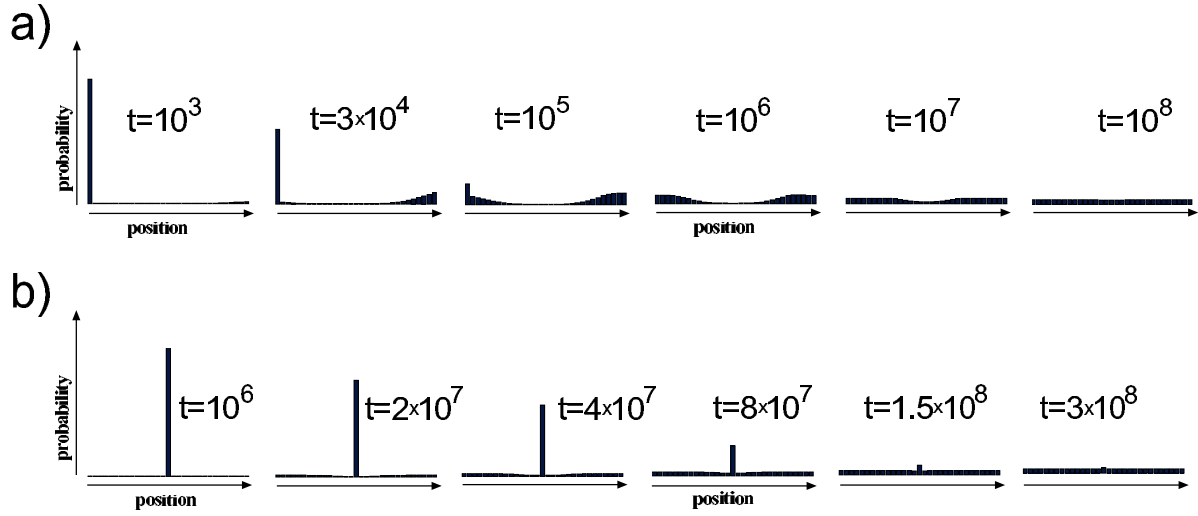


FIG. 9: Relaxation dynamics of two initial states of nucleosome positions on a longer DNA segment (147 + 300 bp): a) end positioned and b) centrally positioned initial species. Note the initial difference in relaxation time scales for a) and b) (which are due to different loop energies involved).

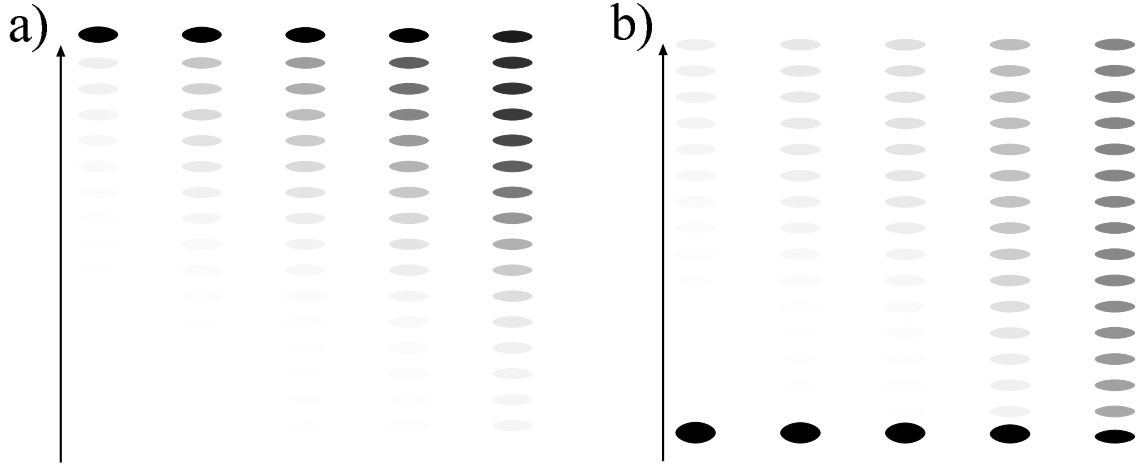


FIG. 10: The (1-D) gelelectrophoresis signatures simulated for the relaxation dynamics of the two initial species from Fig. 9. a) End positioned (lanes 1-5 corresponding to incubation times (1,2,3,10,50) $\cdot 10^4 C_A^{-1}$) and b) centrally positioned (incubation times (1,2,3,10,50) $\cdot 10^6 C_A^{-1}$).

one half to the other.

Hence, the question arises if the repositioning observed in these experiments was facilitated via the loop mechanism or if it occurred via a different process. An analysis of the results is made especially difficult by two complications: (a) the nucleosomes seem to prefer to sit on the ends of the DNA fragments and (b) most of the experiments use strong positioning sequences (like the 5S rDNA sequence). This means that, independent of what the repositioning process might be, the nucleosomes have certain preferred positions and these might obscure the underlying repositioning process.

With regard to this fact, let us consider two other repositioning mechanisms that one could imagine. The first one is that the nucleosome detaches completely from the DNA and attaches at some other position (or even a different DNA molecule). This process, however, seems to be excluded by two facts (among others). First that no repositioning from one half to the other of the 414bp DNA or to competitor DNA fragments was observed [8, 9]. Secondly, once completely detached from the DNA template the histone octamer becomes unstable and disintegrates into a tetrameric and two dimeric subunits which makes an effective nucleosome reconstitution di-

cult.

The other mechanism could be a local screwing motion as already suggested in Ref. [9]. This process would lead to a repositioning with one bp per step. The preponderance of 10bp steps observed for the 5S rDNA experiments could then be explained as being due to the fact that the positioning sequence prefers the nucleosome rotationally positioned on one side of the DNA where it can be easily bent around the octamer. Also 10bps (and even a few multiples of 10bps) apart this effect can still be seen and hence the nucleosome would prefer positions multiples of 10bps apart. To our best knowledge, the experiments to date do not allow to distinguish whether the 10bp repositioning works via small loops or via cork-screwing.

It would be therefore important to perform experiments on DNA pieces that do not provide the nucleosome with a preferred rotational setting. In that case the 10bp footprint should disappear if nucleosomes reposition themselves via cork-screwing. It would also be important to perform experiments with rather long DNA fragments since we expect that large-loop repositioning can be detected in such systems.

Finally, we note that nucleosome repositioning *in vivo* is facilitated via so-called chromatin remodeling complexes, huge multiprotein complexes that harness energy by burning ATP [2, 4, 5]. There are basically two major classes: ISWI and SWI/SNF. The first one seems to induce small scale repositioning which might work via twisting DNA that leads to a corkscrew movement as discussed above. It might, however, also be possible that this complex induces small loops on the nucleosome as recent experiments on nicked DNA suggest [34]. The other class of remodeling complexes seems to induce large loop structures as they have been observed recently via electron spectroscopy [35]. Whatever the details of the functions of these remodeling complexes might be, it is tempting to speculate that they catalyze and direct processes which might even take place when they are not present (like small loop and large loop formation as well as screwing. In this case the computed looping energy (cf. Fig. 5) and repositioning rates might give a first hint about ATP requirements and the dynamics of enzymatic repositioning.

Another interesting and very prominent system known to mediate nucleosome repositioning via loop formation is unexpectedly the ubiquitous RNA-Polymerase (RNA-P). It is found to be able to transcribe DNA through nucleosomes without disrupting their structure, yet moving them upstream the DNA template, i.e., in the opposite direction of transcription [36]. To rationalize this seemingly paradoxical finding Felsenfeld et al. introduced a DNA looping model [36] which assumes that the RNA-P crosses the nucleosome in a loop. This would indeed explain the backwards directionality of repositioning. An interesting question in this context is how our intranucleosomal loops considered above relate to those formed by the RNA-P. Can we say something about the repositioning distance distribution, does the looping energy (Fig. 5)

apply here? The geometry of RNA-P-DNA complex on a nucleosome is certainly different from the simple loop case, as ingoing and outgoing DNA from RNA-P enclose a (rather soft yet) preferential angle of $\sim 100^\circ$ (dependent on RNA-P type, cf. Refs. [37, 38, 39]). The latter facilitates the loop formation as the free DNA has to bend less to fold back onto the octamer surface. Besides the apparent differences from the "naked" intranucleosomal loops problem, a slight generalization of our present model which incorporates the preferential RNA-P "opening" angle can be performed within the same mathematical framework developed here. It would be interesting to compute the resulting nucleosome transfer distance on short and long DNA templates in an analogous manner as performed above. An outcome of such a study could be, for instance, an answer to questions like: what is the highest linear nucleosomal density in polynucleosomal arrays, up to which nucleosomes are not to be removed from the DNA template (due to loop formation and nucleosome transfer prohibited by the neighboring nucleosome) during transcription.

Such fundamental biological questions make a further elaboration of intra-nucleosomal loop theory, its generalization to different loop geometries, and finally its application to different loop creating proteins (SWI/SNF, RNA-P) an intriguing task for future work.

V I. APPENDIX : THE CIRCLE-LINE APPROXIMATION

Although the Kirchhoff's analogy provides us with essentially analytic solutions for the rod deformed in plane, the occurrence of boundary conditions (like Eqs. 5 and 6) prevents us in most cases from obtaining analytical expressions of all the parameters characterizing the solution (like ϕ and m above). To overcome this problem, we suggest here a simple geometric approximation scheme which will prove to be useful in obtaining analytic results for loops within a reasonable accuracy (usually with a deviation of 5-15% from the exact numeric results).

The main idea is the following. The curvature and the energy (Eqs. 17 and 18) of the loop contains the $\text{cn}(j\eta)$ function which for $0 < m < 1$ has the typical oscillatory behavior depicted in Fig. 11 (left). This suggests to approximate the curvature function simply by a step function consisting of an alternating sequence of negative, zero and positive piecewise constant curvatures. Consequently the corresponding rod shape (Fig. 11 right) is approximated by a sequence of circles (positive / negative constant curvature) and lines (zero curvature). An analogous approximation procedure can also be performed in the case $m > 1$ where the cn function has a natural analytical continuation into a dn function with a modified second argument (cf. Ref. [26]).

Using this approximation ansatz several problems concerning planar rods reduce to elementary geometry as seen from the following simple but illustrative examples.

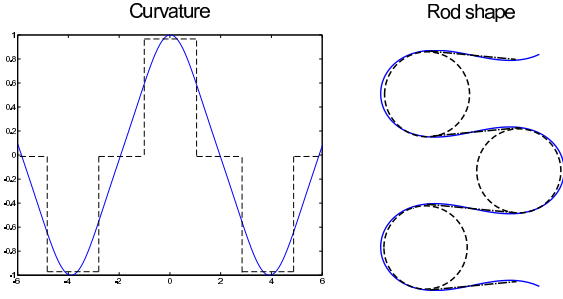


FIG. 11: The circle-line approximation for planar rods. The curvature of an equilibrium rod shape (cn-function, cf. Eq. 17) is approximated by a periodic sequence of step-functions. The latter corresponds to an approximation of the rod shape by a sequence of straight lines ($\kappa = 0$) and circles ($\kappa = \text{const.}$) glued together in a smooth manner (continuous tangents).

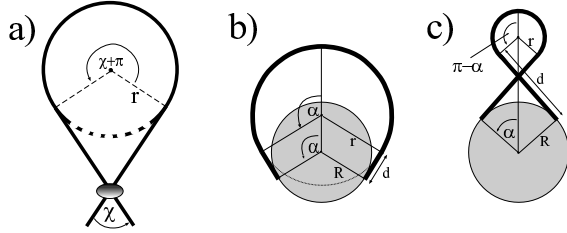


FIG. 12: Three applications of the circle-line approximation: Problems with complex constraints reduce to simple geometries leading to good approximations: a) the Yamakawa-Stockmayer angle b) simple loops and c) crossed loops (see the Appendix text for details).

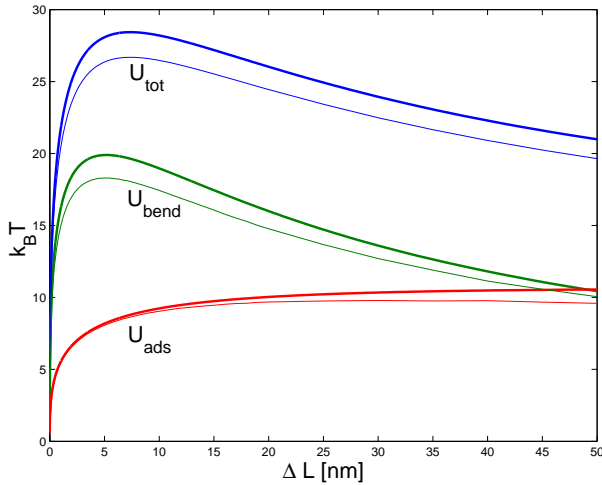


FIG. 13: Comparison of the adsorption and bending energy contributions (U_{ads} and U_{bend}) as well as the total ground state energy U_{tot} of the simple loop. The fat lines represent the circle-line approximation (cf. Eq. 30) whereas the thin lines show the corresponding exact expressions, Eqs. 1 and 20 (thin line). The parameters are $\kappa_{\text{ads}} = 0.7k_B T/\text{nm}$ and $A = 50\text{nm}$, $k_B T$ and $R = 4\text{nm}$.

1) The Yamakawa-Stockmayer angle [29]: Two points on the rod are glued together without restricting the orientation of the tangents, e.g., a protein connects two distant points on DNA (cf. Fig. 12a). What is the preferred angle between the tangents in the ground state of the rod? By imposing a fixed total rod length L we have the simple constraint $L = 2\cot\frac{\chi}{2} + \pi r$ from which we can eliminate r and write the elastic energy of the configuration as $U_{\text{DNA}}^{\text{bend}} = \frac{A}{L} \left(\cot\frac{\chi}{2} + \frac{\pi}{2} \right)$. Its minimization leads to the transcendental condition $\cot\frac{\chi}{2} = \tan\frac{\chi}{2}$ with the only relevant solution $\chi = 77.5^\circ$. The latter angle differs by 5% from the exact result $\chi = 81.6^\circ$ (by Yamakawa and Stockmayer in [29]) which is satisfactory regarding the simplicity of the computation.

2) Simple and crossed loops (Fig. 12 b,c): We can easily derive an approximate energy expression for simple / crossed loops as a function of the excess length L and the opening angle α . By applying simple geometry the excess length constraint can be easily eliminated (the tangency constraint is trivially fulfilled by the ansatz) and we arrive at

$$U_{\text{simple}}(\alpha) = 2A \frac{\tan\frac{\alpha}{2}}{2R(\tan\frac{\alpha}{2})} + R\kappa_{\text{ads}} \quad (30)$$

for simple loops and

$$U_{\text{cross}}(\alpha) = 2A \frac{1 + \tan\frac{\alpha}{2}}{L - 2R(\tan\frac{\alpha}{2})} + R\kappa_{\text{ads}} + U_{\text{def}}(\alpha) \quad (31)$$

for crossed loops where A , R and κ_{ads} defined as above and U_{def} being the excluded volume interaction at the crossing point, which is considered below (and applied in the main text as Eq. 26). We remark that the above expressions for U_{simple} and U_{cross} are valid within certain intervals which are given by the restriction $0 < \alpha < \pi$ and by the condition that the first terms in the brackets of Eqs. 30 and 31 are positive (these are the necessarily positive bending energy contributions in the two cases.)

These fairly simple expressions can now be used in the two cases to obtain explicitly the ground state energies by minimizing Eq. 30 and Eq. 31 with respect to α . For instance, setting $U_{\text{simple}}^0(\alpha) = 0$ we obtain a transcendental equation for α . We can now use the fact that this condition is algebraic in L so that we can solve it for $L = L(\alpha)$. Thus instead of finding $\alpha = \alpha(L)$ (which cannot be given in an explicit form) we obtain explicitly its inverse:

$$\frac{L(\alpha)}{R} = \frac{(2 - \cot\frac{\alpha}{2})G(\alpha) + cH(\alpha)}{1 - \cot\frac{\alpha}{2}} + \frac{q \sqrt{[(2 - \cot\frac{\alpha}{2})G(\alpha) + cH(\alpha)]^2 - 4(1 - \cot\frac{\alpha}{2})G^2(\alpha)}}{1 - \cot\frac{\alpha}{2}} \quad (32)$$

with the abbreviations

$$G(\alpha) = \tan\frac{\alpha}{2} - a$$

$$H(\alpha) = \tan^2\frac{\alpha}{2}$$

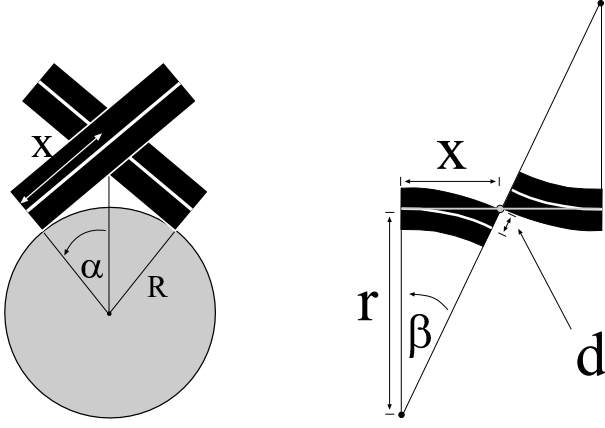


FIG. 14: The out of plane deformation of the incoming/outgoing DNA due to excluded volume in the top projection (left) and seen from the side (right). In the latter case (for the sake of visual clarity) the two rods are depicted in a single plane, i.e., rotated around their contact point (grey dot).

In Eq. 32 the introduced dimensionless constant is $c = 1 + 2R^2 \mu_{\text{ads}} A^{-1}$ ($0 < c < 1$, and $c = 0.69$ here) and is the sign accounting for different branches of the parametrized solution

$$= \begin{cases} 1 & \text{for } 0 \\ 1 & \text{for } =2 \end{cases} \quad =2 \quad m_{\text{ax}}(c) \quad (33)$$

Note that for $=2$ there is only one branch but for > 2 we have two branches⁹ ($=1$) for $L()$. The maximal opening angle $m_{\text{ax}}(c)$ is obtained by setting the discriminant (expression below the square root) in Eq. 32 equal to 0.

From Eq. 32 together with Eq. 30 we obtain an explicit parametric representation of the minimal energy curve for simple loops. A comparison of the approximate minimal energies (Eq. 32 and Eq. 30) with the exact minimal energy (cf. also Fig. 5 for $L < 60\text{nm}$) is shown in Fig. 13. We find that the quantitative agreement is quite satisfactory taking the simplicity of our ansatz into account. We note here that analogous computations as we have shown for simple loops can be performed for crossed loops as well.

For $L \rightarrow 0$ we find after an appropriate expansion of U_{simp} around $= 0$ that the ground state energy scales as $U_{\text{simp}} \propto (L=R)^{1/3}$ in agreement with Ref. [10]. Further we obtain the excess length at which the loop ground state energy is maximal by setting $\partial U_{\text{simp}}() / \partial j = 0$. From this follows the critical length L_{crit} as discussed in the main text (cf. Eq. 24). This simple approximate expression for L_{crit} agrees

within 2-15% with the exact numerical result for a wide range of adsorption energies with deviations becoming larger for adsorption energies above $\mu_{\text{ads}} = 2.0 k_B T = \text{nm}$ (data not shown).

3) The overcrossing potential for crossed loops (Fig. 14): The outgoing DNA path is perturbed out of the plane due to the interaction with the incoming DNA (and vice versa in a symmetrical manner). Because of that our simple planar and phantom model (no self interaction) needs modifications. Instead of solving this (nonplanar) problem within the general theory of self-interacting deformed rods as in Ref. [27] (which is a feasible but rather technical numerical task) we can treat the out-of-plane deformation perturbationally. The first assumption we make here is that the overall shape of the crossed loop does not deviate much from a planar configuration though the orientation of its (effective) plane might be slightly deflected from the nucleosomal plane. Consequently the small perturbation out of the plane and the deformation in plane essentially decouple into a sum of two energy contributions as in Eq. 31. Again by simple geometry (cf. Fig. 13), the second (out of the plane) term in 31 can in first approximation be written as

$$U_{\text{def}}() = \begin{cases} 8 \\ \geq \\ 2A \frac{d \arctan \frac{2dx()}{x^2()d^2}}{x^2()d^2} \end{cases} \text{ for } x() > d$$

$$1 \text{ otherwise} \quad (34)$$

where $d = 1\text{nm}$ is the thickness of DNA and $x() = R \tan$ the length of the crossed segment. In our simple approximation the self-interaction energy diverges for $x \rightarrow d + 0$ as $\frac{1}{2}A(x-d)^{-1}$ (extreme deformation) and approaches zero for $x \rightarrow 1$ as $4A d^2 x^{-3}$ (weak deformation).

We finally note that besides the above given examples it is possible to apply the circle-line approximation to several other standard problems of rod theory like the first and especially the higher order Euler buckling instabilities to obtain qualitatively the known results from buckling theory with very little effort. Thus the circle-line approximation when applied appropriately turns out to be very useful and generally allows computationally inexpensive qualitative and quantitative insights into the behavior of (planar) deformed rods.

VII. ACKNOWLEDGMENTS

We thank S. M. Angenot, R. Bruinsma, W. M. Gelbart, J. Widom and R. Everaers for useful discussions.

⁹ The latter means that for $\alpha = 2$ there are two different excess loop lengths leading to the same (equilibrium) angle, i.e., with increasing L the nucleosome angle opens but after

passing some critical point on the L axis, it starts closing again.

-
- [1] Widom J. 1998. Structure, dynamics, and function of chromatin in vitro. *Annu Rev Biophys Biomol Struct.* 27:285-327
- [2] Komberg R.D. and Y. Lorch. 1999. Twenty-five years of the nucleosome, fundamental particle of the eucaryote chromosome. *Cell* 98:285
- [3] Wolffe A. *Chromatin: Structure and Dynamics* (3rd ed.). Academic Press, ISBN 0127619151 (1999)
- [4] Peterson C.L. 2000. ATP-dependent chromatin remodeling: going mobile. *FEBS Lett.* 476 : 68
- [5] Vignali M., A.H. Hassan, K.E. Neely and J.L. Workman. 2000. ATP-dependent chromatin-remodeling complexes. *Mol. Cell Biol.* 20: 1899
- [6] Beard P. 1978. Mobility of histones on chromosome of simian virus-40. *Cell* 15:955-967
- [7] Spadafora C., P. Oudet and P. Chambon. 1979. Rearrangement of chromatin structure induced by increasing ionic strength and temperature. *Eur. J. Biochem.* 100: 225-235
- [8] Meersseman G., S. Pennings and E.M. Bradbury. 1992. Mobile nucleosomes: a general behavior. *EMBO J.* 11:2951-9.
- [9] Pennings S., G. Meersseman and E.M. Bradbury. 1991. Mobility of positioned nucleosomes on 5S rDNA. *J. Mol. Biol.* 220:101-10.
- [10] Schiessel H., J. Widom, R.F. Bruinsma and W.M. Gelbart. 2001. Polymer reptation and nucleosome repositioning. *Phys. Rev. Lett.* 86: 4414-4417; *Phys. Rev. Lett.* 88 129902
- [11] Polach K.J. and J. Widom. 1995. Mechanism of protein access to specific DNA sequences in chromatin: a dynamic equilibrium model for gene regulation. *J. Mol. Biol.* 254:130-49.
- [12] Anderson J.D. and J. Widom. 2000. Sequence and position-dependence of the equilibrium accessibility of nucleosomal DNA target sites. *J. Mol. Biol.* 296:979-87.
- [13] S. Magenot, private communication.
- [14] Luger K., A.W. Mader, R.K. Richmond, D.F. Sargent and T.J. Richmond. 1997. Crystal structure of the nucleosome core particle at 2.8 Å resolution. *Nature* 389:251-60.
- [15] Hagerman P.J. 1988. Flexibility of DNA. *Annu. Rev. Biophys. Biophys. Chem.* 17:265
- [16] Benham C.J. 1977. Elastic model of supercoiling. *Proc. Natl. Acad. Sci. U.S.A.* 74:2397-401.
- [17] Benham C.J. 1979. An elastic model of the large-scale structure of duplex DNA. *Biopolymers* 18:609-23.
- [18] Le Bret M. 1979. Catastrophic variation of twist and writhing of circular DNA with constraint? *Biopolymers* 18:1709-25.
- [19] Le Bret M. 1984. Twist and writhing in short circular DNAs according to first-order elasticity. *Biopolymers* 23:1835-67.
- [20] Swigon D., B.D. Coleman B.D. and I. Tobias. 1998. The elastic rod model for DNA and its application to the tertiary structure of DNA minicircles in mononucleosomes. *Biophys. J.* 74:2515-30.
- [21] Shi Y.M. and J.E. Hearst. 1994. The Kirchhoff elastic rod, the nonlinear Schrödinger equation, and DNA supercoiling. *J. Chem. Phys.* 101:5186-5200
- [22] Fain B. and J. Rudnick. 1997. Conformations of linear DNA. *Phys. Rev. E* 55:7364
- [23] Fain B. and J. Rudnick J. 1999. Conformations of closed DNA. *Phys. Rev. E* 60:7239
- [24] Schiessel H., J. Rudnick, R. Bruinsma and W.M. Gelbart. 2000. Organized condensation of worm-like chains. *Europhys. Lett.* 51:237-243
- [25] Nizette M. and A. Goriely 1999. Towards a classification of Euler-Kirchhoff laminates. *J. Math. Phys.* 40:2830
- [26] Abramowitz M. and I. Stegun. *Handbook of Mathematical Functions with Formulas, Graphs and Tables*. US Gov. Pr. O. (1972)
- [27] Coleman B.D., D. Swigon and I. Tobias. 2000. Elastic stability of DNA configurations. *Phys. Rev. E* 61:747-70.
- [28] Yamakawa H. *Helical Wormlike Chains in Polymer Solutions*. Springer New York, ISBN 3540629602 (1997)
- [29] Yamakawa H. and W.H. Stockmayer. 1972. Statistical Mechanics of Wormlike Chains II. *J. Chem. Phys.* 57, 2843
- [30] Bouchaud J.P. and A. Georges. 1990. Anomalous diffusion in disordered media - statistical mechanics, models and physical applications. *Phys. Rep.* 195:127
- [31] Klafter J., M.F. Shlesinger and G. Zumofen. 1993. Non-Brownian transport in complex systems. *Chem. Phys.* 177:821
- [32] Sokolov I.M., J.M. Ai and A. Blumen. 1997. Paradoxical diffusion in chemical space for nearest-neighbor walks over polymer chains. *Phys. Rev. Lett.* 79:857
- [33] de Gennes J. and G. Jannick. *Polymers in Solution*. Clarendon Press, Oxford 1990.
- [34] Langst G. and P.B. Becker. 2001. ISWI induces nucleosome sliding on nicked DNA. *Mol. Cell* 8:1085-1092
- [35] Bazett-Jones D.P., J. Cote, C.C. Landel, C.L. Peterson and J.L. Workman. 1999. The SWI/SNF complex creates loop domains in DNA and polynucleosome arrays and can disrupt DNA-histone contacts within these domains. *Mol. Cell Biol.* 19: 1470
- [36] Felsenfeld G., D. Clark and V. Studitsky. 2000. Transcription through nucleosomes. *Biophys. Chem.* 86:231
- [37] Rees A.R., R.W. Keller, J.P. Vesnka, G. Yang and C. Bustamante. 1993. Evidence of DNA bending in transcription complexes imaged by scanning force microscopy. *Science* 260:1646
- [38] Rivetti C., M. Guthold and C. Bustamante. 1999. Wrapping of DNA around the E. coli RNA polymerase open promoter complex. *EMBO J.* 18:4464
- [39] Schulz A., N. Mücke, J. Langowski and K. Rippe. 1998. Scanning force microscopy of E. coli RNA Polymerase holoenzyme complexes with DNA in buffer and air. *J. Mol. Biol.* 283:821